

^{201}Tl SPECT Abnormalities, Documented at Rest in Dilated Cardiomyopathy, Are Related to a Lower Than Normal Myocardial Thickness but Not to an Excess in Myocardial Wall Stress

Nathalie Hassan, MD¹; Jean-Marie Escanyé, PhD¹; Yves Juillière, MD²; Pierre-Yves Marie, MD¹; Nicolas David, MD¹; Pierre Olivier, MD¹; Adey Ayalew, MSc¹; Gilles Karcher, MD¹; Jean-François Stolz, PhD³; and Alain Bertrand, MD¹

¹Department of Nuclear Medicine, Unité Propre de Recherche de l'Enseignement Supérieur—Equipe d'Accueil 3447, Centre Hospitalier Universitaire, Nancy, France; ²Department of Cardiology, Unité Propre de Recherche de l'Enseignement Supérieur—Equipe d'Accueil 3447, Centre Hospitalier Universitaire, Nancy, France; and ³Laboratory of Hematology, Faculty of Medicine, Université Henri Poincaré, Nancy, France

This study was aimed at determining whether the ^{201}Tl SPECT abnormalities documented in patients with dilated cardiomyopathy are related to a local excess in wall stress, which might act against the diastolic perfusion of myocardium. **Methods:** We included 6 healthy volunteers and 7 patients with idiopathic dilated cardiomyopathy who underwent ^{201}Tl SPECT at rest. On a 13-segment division of the left ventricle, indices of wall stress and tension were calculated at end-diastole by applying Laplace's law, with thickness and curvature radii being determined for each segment on 2 orthogonal MRI slices. **Results:** Among all patients, 21 analyzed segments had ^{201}Tl SPECT defects (D+) and 67 had none (D-). Myocardial thickness was lower in D+ (0.88 ± 0.30 cm) than in D- (1.23 ± 0.33 cm, $P = 0.0002$) or in segments from healthy volunteers (0.99 ± 0.15 cm, $P = 0.04$). The index of end-diastolic wall tension was also lower in D+ ($2.5 \pm 1.0 \text{ N} \cdot \text{m}^{-1} \cdot \text{mm Hg}^{-1}$) than in D- ($3.3 \pm 1.1 \text{ N} \cdot \text{m}^{-1} \cdot \text{mm Hg}^{-1}$, $P = 0.02$) or in segments from healthy volunteers ($3.2 \pm 1.2 \text{ N} \cdot \text{m}^{-1} \cdot \text{mm Hg}^{-1}$, $P = 0.04$). Last, the index of end-diastolic wall stress, determined by the ratio of wall tension index to myocardial thickness, was equivalent in D+, in D-, and in segments from healthy volunteers (respectively, 3.0 ± 1.4 , 2.8 ± 1.2 , and $3.2 \pm 1.6 \text{ hN} \cdot \text{m}^{-2} \cdot \text{mm Hg}^{-1}$). **Conclusion:** In patients with dilated cardiomyopathy, the abnormalities documented by ^{201}Tl SPECT at rest are related to a lower than normal wall thickness and not to an excess in wall stress or tension. Therefore, partial-volume effects are likely to induce these abnormalities, and they may be unrelated to any insufficiency of myocardial perfusion.

Key Words: ^{201}Tl ; idiopathic dilated cardiomyopathy; SPECT; MRI; myocardial wall stress

J Nucl Med 2002; 43:451–457

Previous SPECT studies have documented the presence of myocardial perfusion abnormalities in patients with dilated cardiomyopathy (1–4). These abnormalities predominate in regions included in the vertical long-axis plane of the left ventricle (apical, inferior, and anterior regions), and their time evolution parallels that of left ventricular dysfunction, suggesting that they could be related to local excesses in the diastolic wall stress (2,3). Such excesses may, indeed, lead to compression of microvessels and, thus, to a decrease in left ventricular myocardial perfusion (5), which occurs mainly during diastole (6). This study was aimed at analyzing whether the ^{201}Tl SPECT findings at rest in patients with dilated cardiomyopathy are related to segmental variations in left ventricular diastolic wall stress.

MATERIALS AND METHODS

Subjects

We included 6 healthy men (mean age \pm SD, 40 ± 18 y) who had no symptoms and had normal echocardiographic results and 7 patients (6 men, 1 woman; mean age, 56 ± 19 y) who had dilated cardiomyopathy with marked left ventricular dysfunction (mean left ventricular ejection fraction, 0.23 ± 0.06 ; range, 0.17–0.35), had been referred for rest-redistribution ^{201}Tl SPECT, and had no other cause of myocardial disease (no coronary stenosis on a recent angiography examination and no history of myocardial infarction, myopericarditis, systemic hypertension, diabetes mellitus, cor pulmonale, congenital heart disease, or valvular heart disease).

Segmental Determination of Left Ventricular End-Diastolic Wall Stress

Using MRI, we calculated local wall stress at end-diastole on a 13-segment division of the left ventricle (Fig. 1) by applying Laplace's law (7): $(r^{-1} + R^{-1})^{-1} \times P$, where r and R are the principal radii of curvature of the ellipsoid and P is the pressure difference across the surface (Fig. 2). When the surface is a left ventricular wall, P may be considered related to the hydrostatic pressure induced by blood from only the left ventricular cavity

Received Jul. 2, 2001; revision accepted Dec. 19, 2001.
For correspondence or reprints contact: Nathalie Hassan, MD, Service de Médecine Nucléaire, Hôpital de Brabois, rue du Morvan, 54500 Vandoeuvre, France.
E-mail: n.hassan-sebbag@chu-nancy.fr

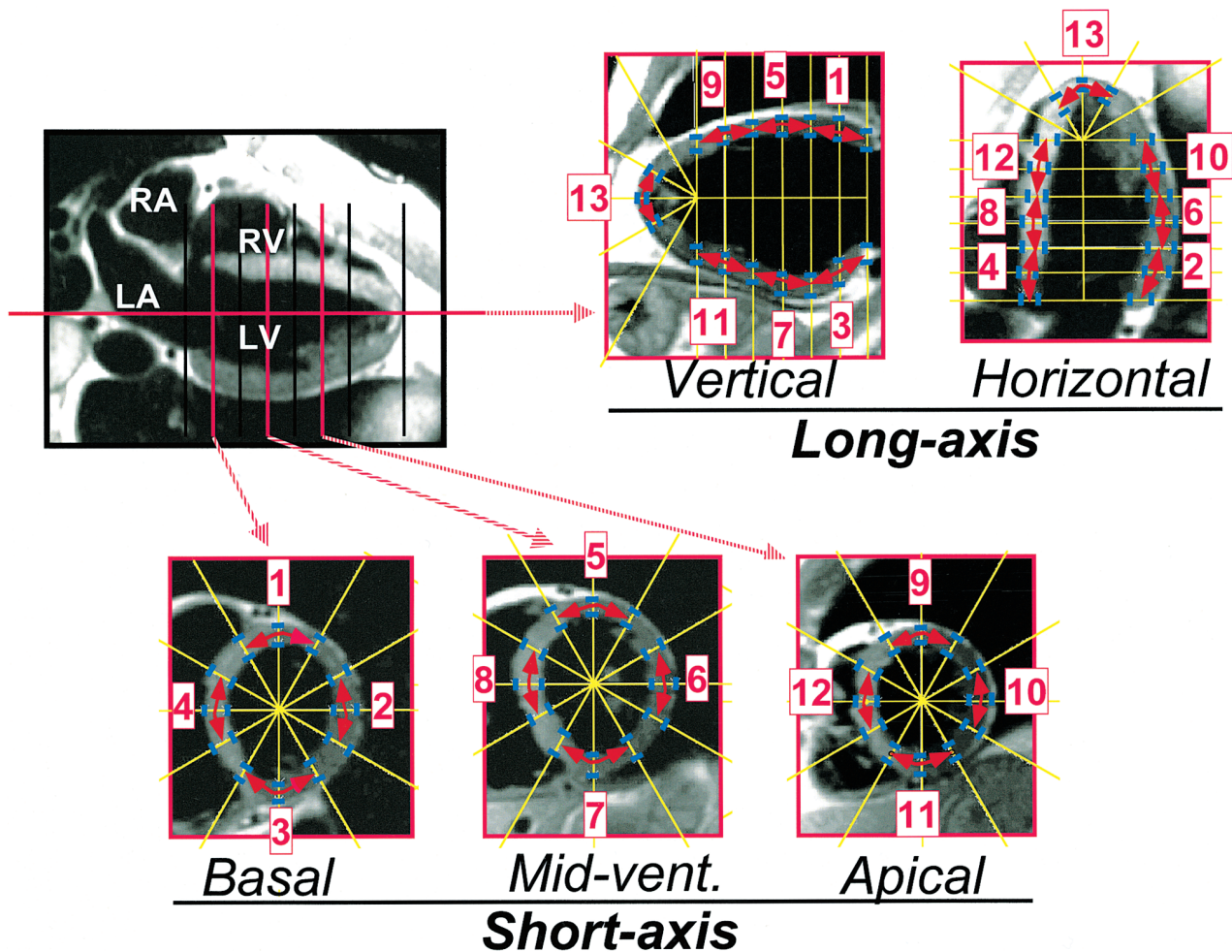


FIGURE 1. Example of MRI slices acquired at end-diastole for healthy volunteer with application of point-positioning software. Epicardial and endocardial borders of left ventricular walls are directed (blue marks) along radial and parallel lines (yellow lines), midwall points being then automatically positioned. For each segment, wall curvature (schematized by red arrows) was determined using coordinates of 3 adjacent midwall points on both orthogonal slices that were used to analyze segment. The 13 left ventricular segments are anterobasal (1), laterobasal (2), inferobasal (3), septobasal (4), anteromedial (5), lateromedial (6), inferomedial (7), septomedial (8), anteroapical (9), lateroapical (10), inferoapical (11), septoapical (12), and apical (13). LA = left atrium; LV = left ventricle; RA = right atrium; RV = right ventricle.

(7,8). However, this pressure was not determined in our study because such a determination would have required invasive cardiac catheterization at the time of MRI. Therefore, we calculated an index of end-diastolic wall tension only, which was expressed per millimeter of mercury of the left ventricular hydrostatic pressure at end-diastole. This parameter, which did not take into account the value of hydrostatic pressure, was sufficient to determine whether the myocardial segments showing defects on SPECT were subjected to a diastolic wall tension higher than that of segments not showing defects on SPECT. Indeed, within the left ventricle, segments with defects and segments without defects are subjected to the same level of hydrostatic pressure.

Finally, the index of end-diastolic wall tension was calculated, for a standard value of 1 mm Hg of the left ventricular hydrostatic pressure at end-diastole, with the formula $0.133 \times (r^{-1} + R^{-1})^{-1}$, where 0.133 is a conversion coefficient to obtain a unit of $N \cdot m^{-1} \cdot mm \text{ Hg}^{-1}$ (9). In addition, an index of end-diastolic wall stress was calculated using the ratio of wall tension index to myocardial thickness (in $N \cdot m^{-2} \cdot mm \text{ Hg}^{-1}$).

MRI Procedure

Local myocardial thickness and curvature radii were calculated from images obtained with a 1.5-T MRI scanner (Signa 1.5; General Electric Medical Systems, Milwaukee, WI) using a recently developed "black blood" fast-spin-echo sequence (10), which allows clear delineation of the left ventricular walls at end-diastole. So that the MRI and SPECT slices would be oriented similarly, pilot MR scans were obtained in the same planes as those used for orientating the SPECT images: multiple slices in the coronal plane, followed by a transverse/sagittal slice in the vertical long axis of the left ventricle and, then, a horizontal long-axis slice. The imaging parameters were a 28- to 34-cm field of view, a 256×128 matrix, an echo train length of 16, a 20-ms echo time, a 500- to 700-ms inversion time, and a 5-mm slice thickness.

Each image was acquired at end-diastole, at the time of the QRS waves on electrocardiography and during a 10- to 15-s breath-hold. Vertical and horizontal long-axis slices crossing the apical extremity of the left ventricular cavity were acquired. The left ventricle was then divided into 4 equal short-axis areas along the vertical

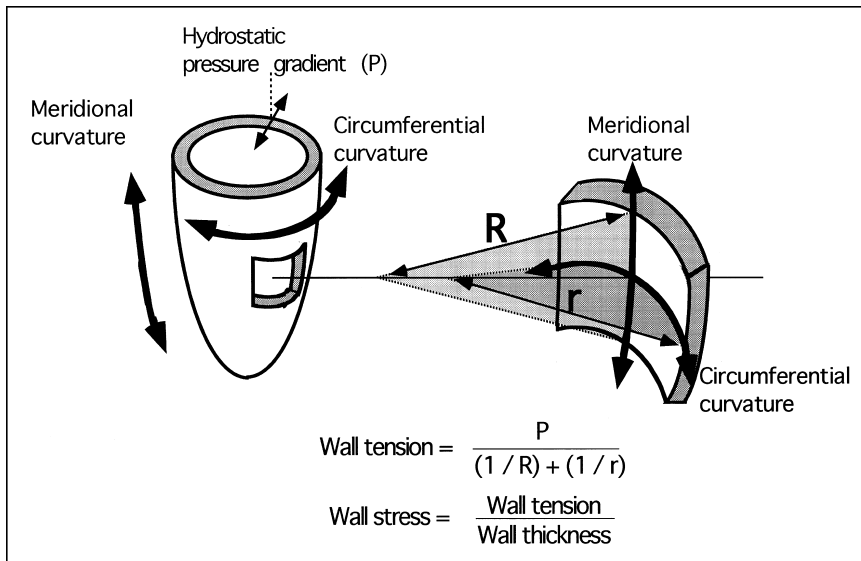


FIGURE 2. Schematic representation of parameters involved in segmental determination of left ventricular wall stress and tension using Laplace's law.

long-axis slice, and a short-axis slice was acquired in the middle of each of the 3 most basal areas (Fig. 1).

Segmental Determination of Myocardial Thickness and Curvature Radii

Each left ventricular segment was analyzed using one orthogonal MRI slice orientated in a meridional direction (vertical or horizontal long-axis slice) and another in a circumferential direction (short-axis slice), except for the apical segments, which were analyzed on both vertical and horizontal long-axis slices (Fig. 1). The images were transferred to a personal computer containing software specially developed to measure myocardial thickness and analyze curvature by positioning points on the ventricular wall.

With the point-positioning software, the borders of the left ventricular walls were directed along radial and parallel lines orthogonal to the walls, as shown in Figure 1. Briefly, 2 points were positioned on each line, one on the epicardial border of the wall and another on the endocardial border of the wall, and myocardial thickness was determined by measuring the distance separating them (a midwall point was also automatically positioned between these 2 points). For each segment, 3 such pairs of points were positioned on the 2 orthogonal slices used to analyze the segment. The thickness of the segment was then calculated by averaging the values from its pairs of points.

The curvature of a segment was also determined for each of the 2 orthogonal slices by calculating the radius of the circle that included the 3 midwall points. According to elementary geometry, the curvature radius of the segment was calculated using:

$$\frac{a \cdot b \cdot c}{4 \sqrt{(s \cdot (s - a) \cdot (s - b) \cdot (s - c))}}$$

where a , b , and c are the distances between the coordinates of the 3 points and s is $(a + b + c)/2$.

SPECT Procedure

Conventional ungated SPECT was performed using a double-head camera (DST-XL; SMV International, Buc, France) 10 min after the rest injection of ^{201}Tl (37 MBq/25 kg of body weight) and after 3–4 h of redistribution. The techniques for imaging, recon-

struction, and visual image analysis were previously described (11). SPECT images were analyzed on the same 13-segment division of the left ventricle as that used for MRI (Fig. 1) and with a 4-point grading scale (0 = normal uptake; 1 = equivocal reduction of uptake; 2 = moderate reduction of uptake; 3 = severe reduction of uptake) (11). Perfusion abnormality at rest was defined as a moderate to severe (>grade 1) reduction in ^{201}Tl uptake on rest SPECT and was considered reversible when the uptake score decreased by ≥ 1 point on redistribution imaging (11).

To assess the partial-volume effect occurring during SPECT, we also applied our acquisition protocol on a phantom consisting of tubes of various diameters (from 0.1 to 25 mm) that contained a constant concentration of ^{201}Tl . The relationship between tube diameter and maximal voxel activity was determined.

Statistical Analysis

Continuous variables were expressed as mean \pm SD, and discrete variables were expressed as percentages. Multiple paired comparisons were performed using the Kruskal–Wallis test, with $P < 0.05$ being considered significant.

RESULTS

Precision and Reproducibility of MRI Measurements

The precision of the MRI measurements was evaluated on a phantom that simulated the shape of a normal heart at end-diastole and had predetermined segment thicknesses and curvatures. Measurement errors were, on average, $2.0\% \pm 1.4\%$ for segment thickness, $3.0\% \pm 2.5\%$ for segment wall tension, and $3.3\% \pm 3.0\%$ for segment wall stress.

To evaluate the reproducibility of the measurements, the MRI parameters were calculated twice, 1 mo apart, in 4 different investigations (52 segments). The differences between the 2 measurements, expressed as a percentage of their average, were $6\% \pm 5\%$ for segment thickness, $11\% \pm 11\%$ for segment wall tension, and $12\% \pm 13\%$ for segment wall stress.

TABLE 1
MRI Variables in Segments from Healthy Volunteers
and in Overall Segments from Patients

Variable	Healthy volunteers (n = 74)	Patients (n = 88)
Thickness (cm)	0.99 ± 0.15	1.12 ± 0.36*
Curvature radii (cm) [†]		
Circumferential	3.2 ± 1.2	4.0 ± 2.0*
Meridional	20 ± 41	11 ± 17*
Diastolic wall tension index [‡] (N · m ⁻¹ · mm Hg ⁻¹)	3.2 ± 1.2	3.1 ± 1.1
Diastolic wall stress index [‡] (hN · m ⁻² · mm Hg ⁻¹)	3.2 ± 1.6	2.9 ± 1.3

**P* < 0.05 for comparisons between overall segments from patients and segments from healthy volunteers.

[†]Apical segments, which are not analyzed using meridional and circumferential curvature radii, are excluded.

[‡]End-diastolic wall tension and wall stress are calculated for standard value of 1 mm Hg of left ventricular hydrostatic pressure at end-diastole.

SPECT Findings

In patients, uptake defects were documented with ²⁰¹Tl SPECT at rest for 22 of the 91 analyzed segments (24%), and 11 were judged to be at least partly reversible at redistribution, with none normalizing completely. Defects at rest were more frequent in the apical (71%), inferior (52%), and anterior (14%) segments (within the vertical long-axis plane of the left ventricle) than in the lateral (5%) and septal (10%) segments.

MRI Findings and Relationship with SPECT Findings

Results from the MRI analysis are detailed in Tables 1 and 2 and are illustrated by an example in Figure 3. Seven segments (3 from patients and 4 from healthy volunteers) were excluded because their borders could not be precisely delineated on MRI slices.

Compared with segments from healthy volunteers, segments from patients had higher curvature radii in the circumferential direction (which is orthogonal to the long axis of the left ventricle) but lower curvature radii in the meridional direction (which parallels the long axis of the left ventricle) (Table 1). Moreover, the patient segments showing uptake defects on ²⁰¹Tl SPECT were markedly thinner than those without defects and were also thinner than the segments from healthy volunteers (Table 2). The index of diastolic wall tension was also lower in the patient segments showing SPECT defects than in the patient segments without defects. This finding was related to the observation that, compared with the patient segments without defects, patient segments with defects had shorter curvature radii in both the circumferential and the meridional directions, though neither difference was significant (respectively, *P* = 0.11 and *P* = 0.06). In addition, no difference in the ratio of wall tension to myocardial thickness, expressing the index of diastolic wall stress, was found between any groups. Last, no significant difference was found when the MRI parameters (listed in Tables 1 and 2) were compared between the segments that showed an at least partial reversibility of the SPECT defects and the segments that did not.

Phantom SPECT Study

The SPECT results for the phantom are given in Figure 4. Because of partial-volume effects, a strong relationship existed between tube diameter and maximal voxel activity. Moreover, a 38% decrease in maximal voxel activity was associated with the decrease in tube size, corresponding to the decrease documented for averaged diastolic myocardial thickness between segments without and segments with SPECT defects (from 12.3 to 8.8 mm).

DISCUSSION

Wall stress, a main determinant of left ventricular function and remodeling, cannot be directly measured within the

TABLE 2
MRI Variables in Segments from Healthy Volunteers and in Patient Segments With and Without ²⁰¹Tl Defects

Variable	Healthy volunteers (n = 74)	Patients	
		No ²⁰¹ Tl defects (n = 67)	²⁰¹ Tl defects (n = 21)
Thickness (cm)	0.99 ± 0.15*	1.23 ± 0.33*	0.88 ± 0.30
Curvature radii (cm) [†]			
Circumferential	3.2 ± 1.2	4.2 ± 1.7	3.3 ± 1.6
Meridional	20 ± 41*	13 ± 21	6 ± 4
Diastolic wall tension index [‡] (N · m ⁻¹ · mm Hg ⁻¹)	3.2 ± 1.2*	3.3 ± 1.1*	2.5 ± 1.0
Diastolic wall stress index [‡] (hN · m ⁻² · mm Hg ⁻¹)	3.2 ± 1.6	2.8 ± 1.2	3.0 ± 1.4

**P* < 0.05 for comparisons with segments that have ²⁰¹Tl SPECT defects.

[†]Apical segments, which are not analyzed using meridional and circumferential curvature radii, are excluded.

[‡]End-diastolic wall tension and wall stress were calculated for standard value of 1 mm Hg of left ventricular hydrostatic pressure at end-diastole.

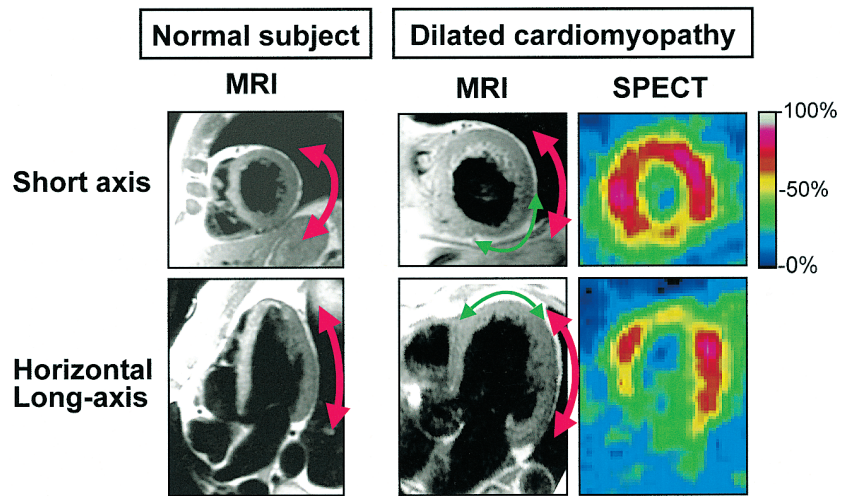


FIGURE 5. Schematic representation of global meridional and circumferential left ventricular curvatures in healthy volunteer and in patient with dilated cardiomyopathy and of segmental curvatures within patient segments showing SPECT defects. Compared with left ventricular walls from healthy volunteer, those from patient are less curved in circumferential direction (red arrows on short-axis slices) but more curved in meridional direction (red arrows on long-axis slices). In addition, in patient segments showing SPECT defects, walls are more curved (green arrows) and thinner than in other segments from this patient.

sion abnormalities of patients with dilated cardiomyopathy were unrelated to any local excess in left ventricular wall stress at end-diastole. However, we also found that these abnormalities were in segments where thickness was, on average, 28% lower than in the other segments, thereby explaining the presence of ^{201}Tl SPECT defects.

Indeed, because of partial-volume effects, SPECT is known to underestimate the concentration of radioactivity in small structures. To illustrate this point, we applied our protocol for cardiac SPECT acquisition to tubes of various diameters containing a constant concentration of ^{201}Tl . Under such conditions, a 38% decrease in maximal voxel activity was associated with a decreased tube size, corresponding to the decrease documented for averaged diastolic myocardial thickness between segments without and segments with SPECT defects. This finding indicates that the magnitude of the partial-volume effect on patient SPECT images was dramatic, but the precise degree of that magnitude is not known because myocardial walls are of far more complex shape than are cylindrical tubes. Nevertheless, these data from the phantom strongly support our observation that, for SPECT performed on patients with dilated cardiomyopathy, a decreased level of ^{201}Tl uptake reflects mainly a decreased mass of myocardial tissue and may therefore be unrelated to any insufficiency of myocardial perfusion.

The segments with ^{201}Tl SPECT defects were thinner than those from healthy volunteers. A possible explanation is that such segments correspond to the areas of myocardial fibrotic involution already documented in patients with dilated cardiomyopathy (14). In these patients, however, the SPECT abnormalities are known to decrease when left ventricular function improves (3); thus, irreversible fibrosis is not a satisfactory explanation and additional mechanisms likely play a role. One additional mechanism could be a lower contractility of the abnormally thin segments, leading to a much lower segment thickness (compared with the other segments) during systole and, thus, to a further decrease in the uptake recorded by conventional ungated

SPECT within these segments. Another mechanism could be a higher photon attenuation, because SPECT defects are predominantly in areas (especially the inferior and apical walls (15)) known to be subjected to a high level of such attenuation. The impact of these additional mechanisms remains to be determined.

Previous studies have shown that, in idiopathic cardiomyopathy, the left ventricle is remodeled from the normal elliptic shape to one more spheric (16,17). This remodeling is caused by both an increased curvature radius in the circumferential direction and a decreased curvature radius in the meridional direction (16,17), as shown in Figure 5. In this study, similar results were documented with MRI, but at the level of a local segmental analysis. However, as Figure 5 illustrates, the thin segments showing SPECT defects were also more curved than were the other segments. This additional remodeling may be related to a bending of thin segments under the force of the pressure arising from the blood cavity. Whatever the mechanism, our results show that this shortening of curvature radii leads to a lowering of the wall tension applied to the surface of the abnormally thin segments, thereby protecting their myocardial diastolic perfusion from any excess in diastolic wall stress or tension.

CONCLUSION

In patients with dilated cardiomyopathy, the abnormalities documented by ^{201}Tl SPECT at rest are related to a lower than normal wall thickness and not to an excess of myocardial wall stress or tension. Therefore, partial-volume effects are likely to induce these abnormalities, and they may be unrelated to any insufficiency of myocardial perfusion.

ACKNOWLEDGMENTS

The authors thank Cécile Tettoni and Arnaud Chauderlot, who developed the point-positioning software, and Jean-

Marc Gravier and Henri Boutelet, who provided precious help with image analysis.

REFERENCES

1. Doi Y, Chikamori T, Takata J, et al. Prognostic value of thallium-201 perfusion defects in idiopathic dilated cardiomyopathy. *Am J Cardiol.* 1991;67:188–193.
2. Juillière Y, Marie PY, Danchin N, et al. Radionuclide assessment of regional difference in left ventricular wall motion and myocardial perfusion in idiopathic cardiomyopathy. *Eur Heart J.* 1993;14:1163–1169.
3. Juillière Y, Marie PY, Danchin N, et al. Serial evaluation of dilated cardiomyopathy with exercise thallium-201 tomography: correlation with the evolution of left ventricular parameters. *Int J Cardiol.* 1994;46:159–167.
4. Chikamori T, Doi YL, Yonezawa Y, Yamada M, Seo H, Ozawa T. Value of dipyridamole thallium-201 imaging in noninvasive differentiation of idiopathic dilated cardiomyopathy from coronary artery disease with left ventricular dysfunction. *Am J Cardiol.* 1992;69:650–653.
5. Hirota Y, Shimizu G, Kaku K, Saito T, Kino M, Kawamura K. Mechanisms of compensation and decompensation in dilated cardiomyopathy. *Am J Cardiol.* 1984;54:1033–1038.
6. Beyar R, Sideman S. Dynamic interaction between myocardial contraction and coronary flow. *Adv Exp Med Biol.* 1997;430:123–137.
7. Wong AYK, Rautaharju PM. Stress distribution within the left ventricular wall approximated as a thick ellipsoidal shell. *Am Heart J.* 1968;75:649–662.
8. Yin FG. Ventricular wall stress. *Circ Res.* 1981;49:829–842.
9. Delepine S, Furber A, Balzer P, et al. MRI quantification of regional variations of left ventricular parietal stress in normal subjects [in French]. *Arch Mal Coeur Vaiss.* 1999;92:1189–1196.
10. Simonetti OP, Finn JP, White RD, Laub G, Henry DA. “Black blood” T2-weighted inversion-recovery MR imaging of the heart. *Radiology.* 1996;199:49–57.
11. Marie PY, Karcher G, Danchin N, et al. Thallium-201 rest-reinjection and iodine-123-MIHA imaging of myocardial infarction: analysis of defect reversibility. *J Nucl Med.* 1995;36:1561–1568.
12. Hayashida W, Kumada T, Nohara R, et al. Left ventricular wall stress in dilated cardiomyopathy. *Circulation.* 1990;82:2075–2083.
13. Fujita N, Duerinckx AJ, Higgins CB. Variation in left ventricular wall stress with cine magnetic resonance imaging: normal subjects versus dilated cardiomyopathy. *Am Heart J.* 1993;125:1337–1345.
14. Ritchie JL, Clarke LJ, Reichenbach D. Congestive cardiomyopathy with segmental wall motion abnormalities and a non-uniform pattern of fibrosis. *Cathet Cardiovasc Diagn.* 1979;5:283–287.
15. Miles J, Cullom SJ, Case JA. An introduction to attenuation correction. *J Nucl Cardiol.* 1999;6:449–457.
16. Douglas PS, Morrow R, Ioli A, Reichek N. Left ventricular shape, afterload and survival in idiopathic dilated cardiomyopathy. *J Am Coll Cardiol.* 1989;13:311–315.
17. Hall S, Cigarrao C, Marcoux L, Risser RC, Grayburn P, Eichhorn EJ. Time course of improvement in left ventricular function mass and geometry in patient with congestive heart failure treated with beta-adrenergic blockade. *J Am Coll Cardiol.* 1995;25:1154–1161.

